Int. J. Electrochem. Sci., 15 **(2020)** 8990 – 9002, doi: 10.20964/2020.09.60

International Journal of
ELECTROCHEMICAL
SCIENCE
www.electrochemsci.org

Enhanced Electrochemical Performance of $LiNi_{0.8}Co_{0.1}Mn_{0.1}O_2$ Cathode Material for lithium ion batteries by WO_3 surface coating

Cong Xiong[1], *Haikou Fu*[2,*], *Lijue Wu*[2], *Gaoqing Yuan*[1,*]

[1] Key Laboratory of Functional Molecular Engineering of Guangdong Province, School of Chemistry and Chemical Engineering, South China University of Technology, Guangzhou 510640, China
[2] Qingyuan Jiazhi New Materials Research Institute Co. Ltd., Qingyuan 511517, China
[*]E-mail: gqyuan@scut.edu.cn (G. Yuan); fuhaikuo@jianae.com (H. Fu)

Received: 6 May 2020 / *Accepted:* 14 July 2020 / *Published:* 10 August 2020

$LiNi_{0.8}Co_{0.1}Mn_{0.1}O_2$ cathode material was successfully modified by using a wet-chemical route to coat WO_3. The microstructures, morphologies, crystal structures, elemental distributions and ionic valence of the prepared cathode materials were carefully analyzed by SEM, EDS, TEM, HRTEM, XRD and XPS. The results indicated that the surface of $LiNi_{0.8}Co_{0.1}Mn_{0.1}O_2$ was uniformly covered by WO_3 particles, and a small amount of W^{6+} could enter to the lattice of $LiNi_{0.8}Co_{0.1}Mn_{0.1}O_2$. The WO_3 coating could prohibit the corrosion of HF and some side reactions for the cathode material during long cycles, thus greatly improving the electrochemical performance and the structural stability of $LiNi_{0.8}Co_{0.1}Mn_{0.1}O_2$. Among the examined $LiNi_{0.8}Co_{0.1}Mn_{0.1}O_2$ cathode materials, 1.0 wt% WO_3-coated $LiNi_{0.8}Co_{0.1}Mn_{0.1}O_2$ has the best initial discharge capacity (185.1 mAh g^{-1}) and an excellent capacity retention (93.2%) after 100 cycles at 1 C.

Keywords: Lithium-ion batteries; $LiNi_{0.8}Co_{0.1}Mn_{0.1}O_2$; WO_3 coating; electrochemical performance

1. INTRODUCTION

With the rapid development in global electric vehicles, it is extremely important to exploit lithium-ion batteries with high capacity, long cycle life and relatively low cost. The cost and capacity of lithium-ion batteries are largely dependent on cathode materials [1]. Ni-rich cathode material is preferentially considered for lithium-ion batteries in electric vehicles because of its advantages of high capacity, relatively low cost and low toxicity [2, 3]. Now, $LiNi_{0.8}Co_{0.1}Mn_{0.1}O_2$ (NCM811) has entered the commercialization stage, but the poor processing performance and poor cycle stability limit its large-scale commercial application. These shortcomings are mainly caused by the following reasons. firstly, the radius of Li^+ and Ni^{2+} is very close, and during the charging and discharging process the nickel atom

will occupy the position of the lithium atom, resulting in cations mixing and capacity loss [4, 5]. Secondly, NCM811 has small amounts of Li_2O and LiOH on its surface, which could react with CO_2 and H_2O from air to generate lithium carbonate and other lithium salts, followed by the reaction with Ni^{4+} to cause structural damage [6, 7]. In particular, impurities on the surface of NCM811 could react with electrolytes during long charge-discharge cycles, and the cathode material would be corroded by HF generated from the electrolyte decomposition, destroying the structural stability of the cathode materials [8].

To solve the above-mentioned shortcomings, some methods (such as surface coating, ionic doping [9-12], control of particle morphologies [13, 14]) have been applied to modify NCM811. The surface coating is currently a widely used and effective method. The common coating materials mainly include metal oxides (such as Al_2O_3 [15], V_2O_5 [16], MgO [17], TiO_2 [18], ZrO_2 [19], MoO_3 [20] etc.), conductive polymers (such as polyaniline [21], polypyrrole [22]), phosphates (such as $AlPO_4$ [23], Li_3PO_4 [24] etc.) and fluorides (such as NH_4F [25], AlF_3 [26], CaF_2 [27] etc.), and ultra-thin $LiAlO_2$ film [28]. The surface coating can act as a stable protective layer for the cathode material to avoid direct contact of the material with electrolytes and reduce occurrence of side reactions, thus improving the structural stability of the cathode material.

WO_3 is an acidic oxide with strong resistance to corrosion of HF and a good conductivity (1.76 S cm^{-1}) [29]. Additionally, WO_3 has a certain reaction activity with lithium, which favors to remove some alkali residues on the surface of Ni-rich cathode material. The advantages of WO_3 as the modified material have aroused interest of researchers. Recently, some researchers used WO_3 to modify various Ni-containing cathode materials, including $Li_{1.2}Ni_{0.2}Mn_{0.6}O_2$ [30], $LiNi_{0.6}Co_{0.2}Mn_{0.2}O_2$ [31] and $LiNi_{0.8}Co_{0.1}Mn_{0.1}O_2$ [32]. These investigations reveal that the WO_3 coating layer could effectively improve the electrochemical performances and structure stability of Ni-containing cathode materials. However, as for $LiNi_{0.8}Co_{0.1}Mn_{0.1}O_2$ cathode material, the surface modification by WO_3 (0.25 wt%) only enhanced 5.88% of retention capacity from 81.19 % to 87.02% after 100 cycles in the potential range of 2.8–4.3 V at 1 C rate [32]. Therefore, it is still highly desired to enhance efficacy of WO_3 as the modified material through developing surface-coating methods. In this work, WO_3 was uniformly coated on the surface of $LiNi_{0.8}Co_{0.1}Mn_{0.1}O_2$ via a wet-chemical coating route. At the same time, a small amount of W^{6+} could penetrate to the lattice of $LiNi_{0.8}Co_{0.1}Mn_{0.1}O_2$.

Our investigation indicates that 1wt % WO_3 surface-coating could significantly enhance the electrochemical properties and cycling stability of $LiNi_{0.8}Co_{0.1}Mn_{0.1}O_2$ cathode material. The 1.0 wt% WO_3-coated $LiNi_{0.8}Co_{0.1}Mn_{0.1}O_2$ has a high initial discharge capacity (185.1 mAh g^{-1}), and its capacity retention is obviously improved from 81.6% to 93.2% after 100 cycles at 1 C, demonstring its potential application.

2. EXPERIMENTAL

2.1 Material Preparation

A certain amount of commercial $Ni_{0.8}Co_{0.1}Mn_{0.1}(OH)_2$ precursor was mixed uniformly with LiOH-H_2O (Li/TM molar ratio at 1.05, M = Ni, Co and Mn) in an agate mortar. The homogeneous mixture was first heated at 480 °C for 5 h and then calcined at 750 °C for 16 h in oxygen atmosphere. After triturating and sieving, $LiNi_{0.8}Co_{0.1}Mn_{0.1}O_2$ (NCM811) power was obtained.

The preparation process of WO_3 coated NCM811 is shown in Fig. 1. A certain amount of tungsten acid was dissolved in 30 mL ammonia aqueous solution to form deposite, followed by adding the as-prepared NCM811. The obtained suspension was dispersed by sonication for 15 min, and then was heated at 90 °C under magnetic stirring conditions until the solvent (H_2O) was completely evaporated. The obtained solid product was transferred to a petri dish and put into an oven at 80 °C to dry for 12 h. The dried product was calcined at 600 °C for 3 h in air. Finally, WO_3-coated NCM811 sample was obtained. The coating amount of WO_3 was controlled to 0.5 wt%, 1 wt% and 2 wt%, marked as W-0.5, W-1.0 and W-2.0, respectively. The pure WO_3 was synthesized by the same method without the addition of NCM811 powder.

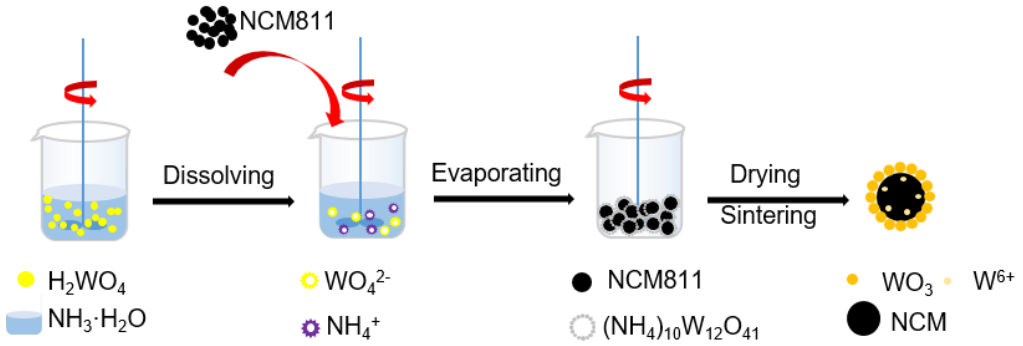

Figure 1. Illustration process of the preparation of WO_3-coated $LiNi_{0.8}Co_{0.1}Mn_{0.1}O_2$ (WO_3-coated NCM811) cathode materials.

2.2 Materials Characterization

XRD patterns were determined by an X-ray diffraction equipment (XRD) with Cu-K_α radiation source in the scanning range of 10°~80°. The morphologies of the prepared samples were characterized by scanning electron microscopy (SEM) with energy dispersive X-ray spectroscopy (EDS) (S4800, Hitachi, Japan), and transmission electron microscopy (TEM, JEM-2100F, JEOL). In addition, the elemental composition was determined by using an X-ray photoelectron spectroscopy (XPS, 250xi, Thermo ESCALAB).

2.3 Electrochemical Measurements

The prepared cathode materials were used to resemble CR2032 coin cells for testing their electrochemical performances. The preparation of working cathode (positive electrode) underwent a series of procedures as follows. In a high-speed mixer (AR 100, THINKY, Japan), the active cathode material (80 wt%) was first mixed with acetylene black (10 wt%) and polyvinylidene fluoride (10 wt%) in *N*-methyl-2-pyrrolidone, and then the mixture was stirred for 5 min at 2000 rpm. The obtained slurry mixture was pasted onto an aluminum foil and dried in vacuum at 100 °C for 12 h. The working cathode with a diameter of 14 mm was finally obtained by cutting the coated aluminum foil. The electrolyte solution consists of 1 M $LiPF_6$ and a mixing solvent (ethylene carbonate, ethyl methyl carbonate and dimethyl carbonate with a volume ratio of 1:1:1). The charge-discharge cycling was carried out at 1.0 C

(180 mA g^{-1}), under the cut-off potential from 2.7 to 4.3 V at 27 °C by using a Neware battery test system. Electrochemical impedance spectroscopy (EIS) was determined within a frequency range of 0.01 Hz to 0.1 MHz. Cyclic voltammetry (CV) test was performed with 0.1 mV s^{-1} scan rate.

3. RESULTS AND DISCUSSION

XRD patterns of the prepared WO_3 are shown in Fig. 2a. All the diffraction peaks are corresponded to with the WO_3 phase (JCPDS Card: 72-0677), and no additional impurity diffraction peaks are observed, indicating that pure WO_3 can be obtained via the present method.

In Fig. 2b, all the prepared cathode materials exhibit a hexagonal α-$NaFeO_2$ structure of R-3m space group, which implies that a small amount of WO_3 coating does not destroy the layered structure of $LiNi_{0.8}Co_{0.1}Mn_{0.1}O_2$. The distinct (006/102) and (108/110) cleavage peaks can be observed, further indicating that these materials have well-developed layered structure [33]. The WO_3-coated NCM811 has no diffraction peaks corresponding to WO_3 in the XRD pattern, which may be due to the WO_3 coating beyond the detection limit of XRD. In the magnification plot of the (003) peak, the peak shift in W-0.5 coated NCM811 could be not observed, which may be attributed to the coating amount of WO_3 being too low. For W-2.0 coated NCM811, the peak shift is not appeared as well, which may be ascribed to the fact that the excessive coating of WO_3 could not be uniformly spread over the surface of NCM811, making tungsten ions difficultly penetrate to the lattice. It is worthy to note that the (003) peak of W-1.0 coated NCM811 is shifted towards the left, demonstrating that part of W^{6+} species are resided in the layered lattice of NCM811, resulting in a wider lattice spacing [9]. This may favor to form a wider lithium ion transport channel that can transport lithium ions faster in the W-1.0 coated NCM811. In addition, Table 1 lists the lattice parameters obtained based on the XRD results of the samples. Although the *a* and *c* of the modified samples become slightly larger compared to NCM811, their *c*/*a* values are all above 4.9, indicating that these samples have a good crystallinity and laminar structure. When the value of I(003)/I(104) is more than 1.2, it is generally considered that the mixing degree of cations in the nickel-rich material could meet practical requirements. Notably, the value of I_{003}/I_{104} appeared a decreasing trend with increasing WO_3 coated, so the coating amount of WO_3 should be well controlled [34].

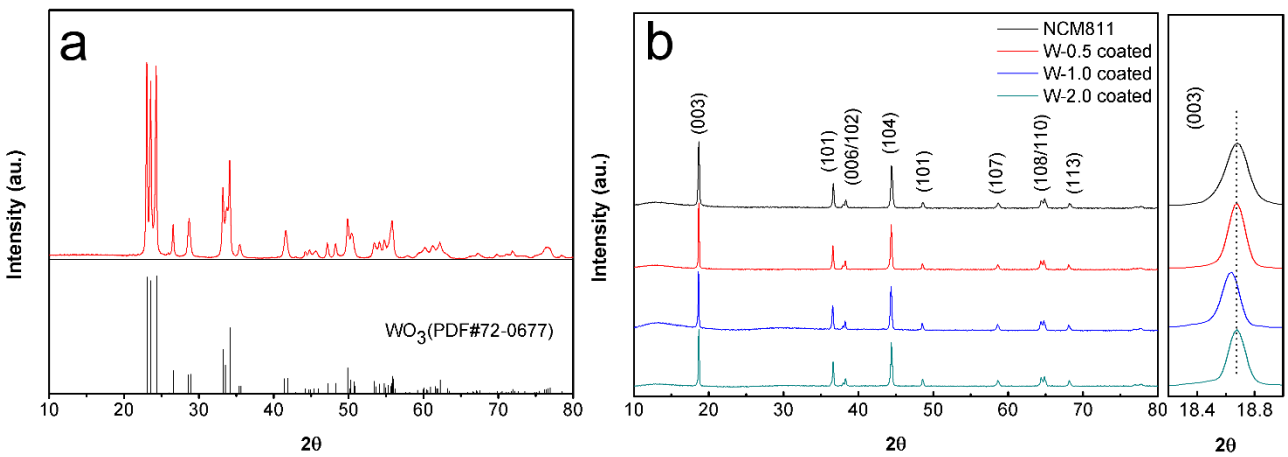

Figure 2. XRD patterns of (a) WO_3, (b) NCM811 and WO_3-coated NCM811 samples.

Table 1. Lattice parameters, *c*/*a* and I (003)/I (104) values of the samples.

Sample	*a*(Å)	*c*(Å)	*c*/*a*	I (003)/I (104)
NCM811	2.8722	14.2027	4.9449	1.515
W-0.5 coated	2.8750	14.2062	4.9413	1.490
W-1.0 coated	2.8744	14.2074	4.9428	1.381
W-2.0 coated	2.8730	14.2098	4.9460	1.341

Fig. 3 shows the SEM images of NCM811 and WO_3-coated NCM811 samples, and all the samples consist of sphere-like particles of about 12 μm in diameter, which mean that the WO_3 coating does not change the morphologies of NCM811 particles. In Fig. 3f-h, the surface of NCM811 was relatively smooth, while the surface of WO_3-coated NCM811 samples became rough. The excess coated-amount of WO_3 would lead to uneven dispersion on the surface of NCM811 particles, and tungsten ions would difficultly penetrate to the lattice of NCM811. To further confirm WO_3 coated on the surface of NCM811, EDS tests were performed on W-1.0 coated NCM811. As shown in Fig. 4b-e, Ni, Co, Mn and W elements are homogeneously distributed over the surface of NCM811, proving that WO_3 is successfully coated on the surface of NCM811.

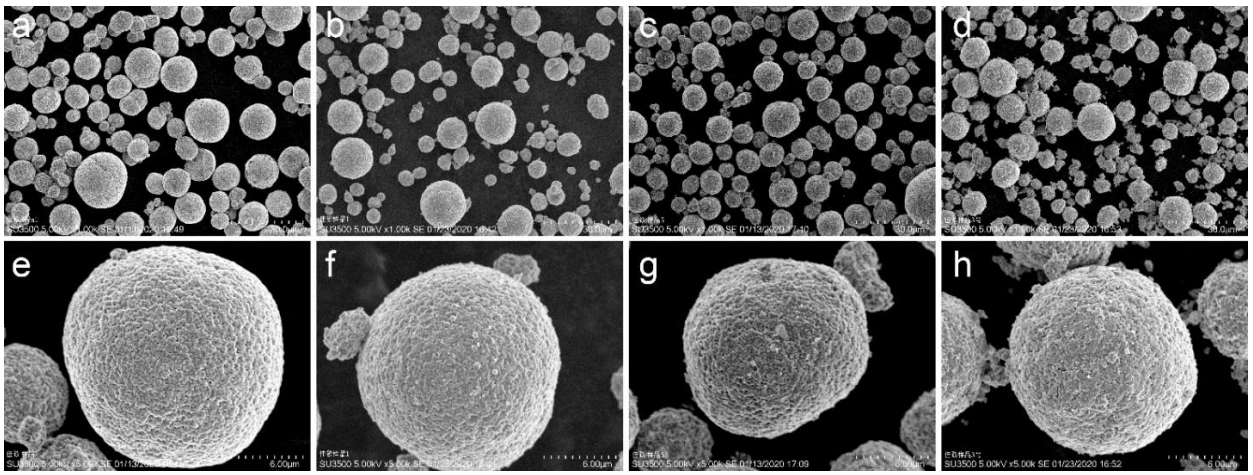

Figure 3. SEM images of NCM811 (a, e), W-0.5 coated (b, f), W-1.0 coated (c, g), and W-2.0 coated NCM811 (d, h).

To further observe the differences in surface morphology and microstructure between NCM811 and W-1.0 coated NCM811, TEM and HRTEM analyses were applied, as shown in Fig. 5. The TEM results (Fig. 5a and b) show that the NCM811 particles have very smooth edges, while the W-1.0 coated NCM811 particles display relatively rough edges with the modified traces.

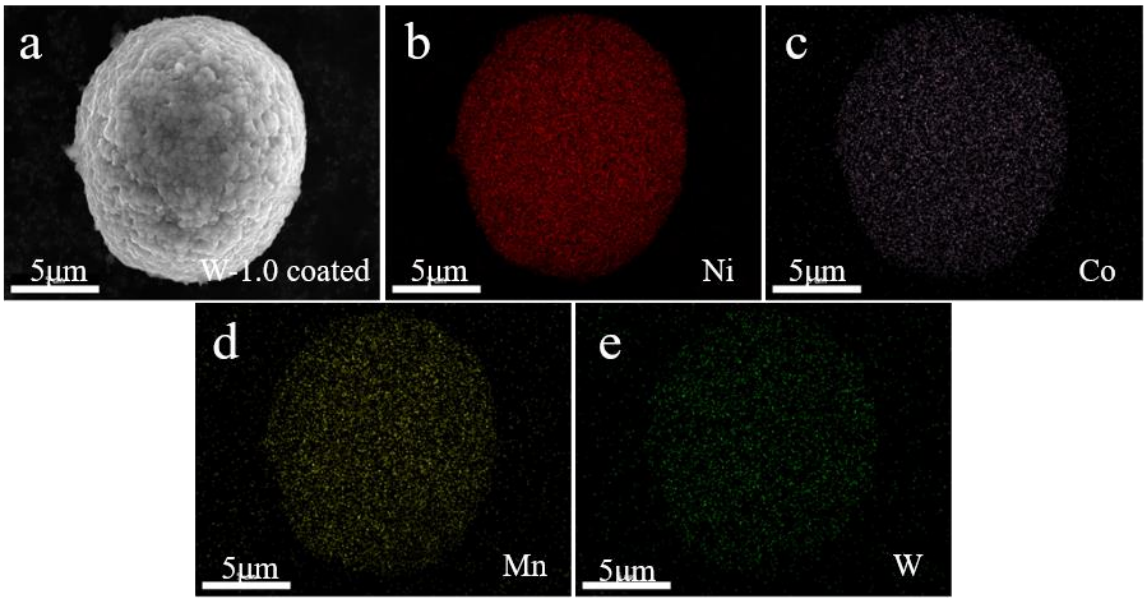

Figure 4. (a) SEM images of W-1.0 coated NCM811 and (b-e) EDS mapping patterns of Ni, Co, Mn and W.

The HRTEM images of NCM811 and W-1.0 coated NCM811, and the their corresponding FFT (fast Fourier transformed) and IFFT(inverse fast Fourier transformed) images of the selected regions, were illustrated in Fig. 5c and d, respectively. In the NCM811 case (Fig. 5c), only one layer of lattice structure could be observed, and the IFFT image of the selected region shows that the lattice streaks are well ordered with an interlunar spacing of 0.237 nm, corresponding to the (006) crystal planes of NCM811.

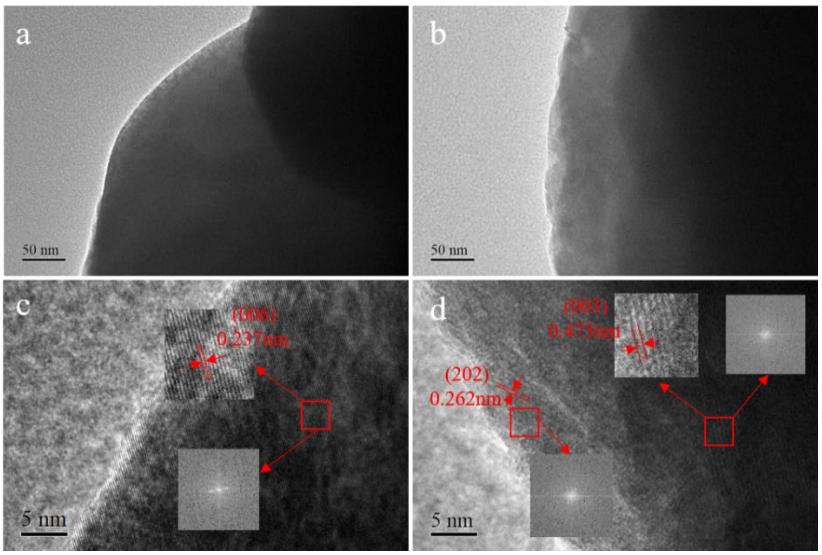

Figure 5. TEM and HRTEM images of (a, c) NCM811 and (b, d) W-1.0 coated NCM811; the insets in (c) and (d) corresponding to FFT and IFFT images of the selected region.

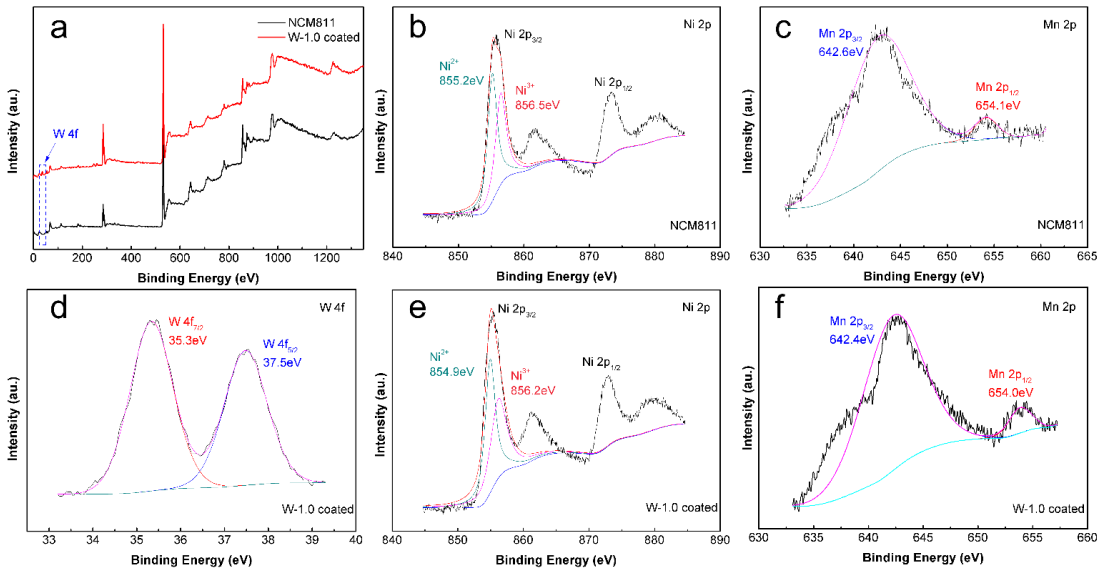

Figure 6. XPS spectra of NCM811 and W-1.0 coated NCM811.

In the W-1.0 coated NCM811 case (Fig. 5d), two lattice structures with different lattice orientation and lattice spacing exist. The measured interlunar spacing is 0.437 and 0.262 nm which correspond to the (003) crystal plane of NCM811 and the (202) crystal plane of WO_3, respectively [35]. From Fig. 5d, it could be seen that WO_3 is tightly coated on the surface of NCM811, and the thickness of the coated layer is around 15-20 nm.

The XPS spectra of NCM811 and W-1.0 coated NCM811 were further analysed. As shown in Fig. 6a, the full spectra of NCM811 and W-1.0 coated NCM811 have a very similar shape. It should be noted that the full spectra of W-1.0 coated NCM811 have a distinct peak of W 4f near 35 eV, whereas NCM811 does not. Fig. 6d shows the original peak of W 4f and its fitted peak. It could be seen that the binding energies of W $4f_{5/2}$ and W $4f_{7/2}$ are 37.5 eV and 35.3 eV, respectively, which correspond to the typical peaks of WO_3 [36]. This result further confirmed that the WO_3 coating was successful. In addition, the measured XPS corresponding to Ni and their fitted XPS obtained by XPSPEAK software are shown in Fig. 6b and e. All the fitted lines (red lines) are matched well with the measured lines (black lines), indicating that the fitting results are reasonable. The peaks of Ni^{2+} and Ni^{3+} in NCM811 are located at 855.2 eV and 856.2 eV respectively, while the corresponding peaks of W-1.0 coated NCM811 appear at 855.0 eV and 856.0 eV, which are good in agreement with the previous report [37]. This means that the layer structure of W-1.0 coated NCM811 is not changed significantly. By comparing the fitting curves of the two samples, it was found that the content of Ni^{2+} and Ni^{3+} in the samples was different and the number of Ni^{3+} on the surface of W-1.0 coated NCM811 was less than that of NCM811, indicating that the WO_3 modification changed the distribution of valent states of nickel on the surface of NCM811. The peaks at 642.5 eV and 654.2 eV in Fig. 6c belong to Mn $2p_{3/2}$ and Mn $2p_{1/2}$ of NCM811, while the corresponding peaks in the W-1.0 coated NCM811 at 642.6 eV and 654.2 eV (Fig. 6f), respectively. These results indicate that the positive tetravalent state of Mn could be kept before and after the WO_3 modification. Owing to the decrease in Ni^{3+} content of W-1.0 coated NCM811, W^{6+} would penetrate into the crystals of the cathode material to maintain the electroneutrality, making the layer spacing of the cathode material become larger [38].

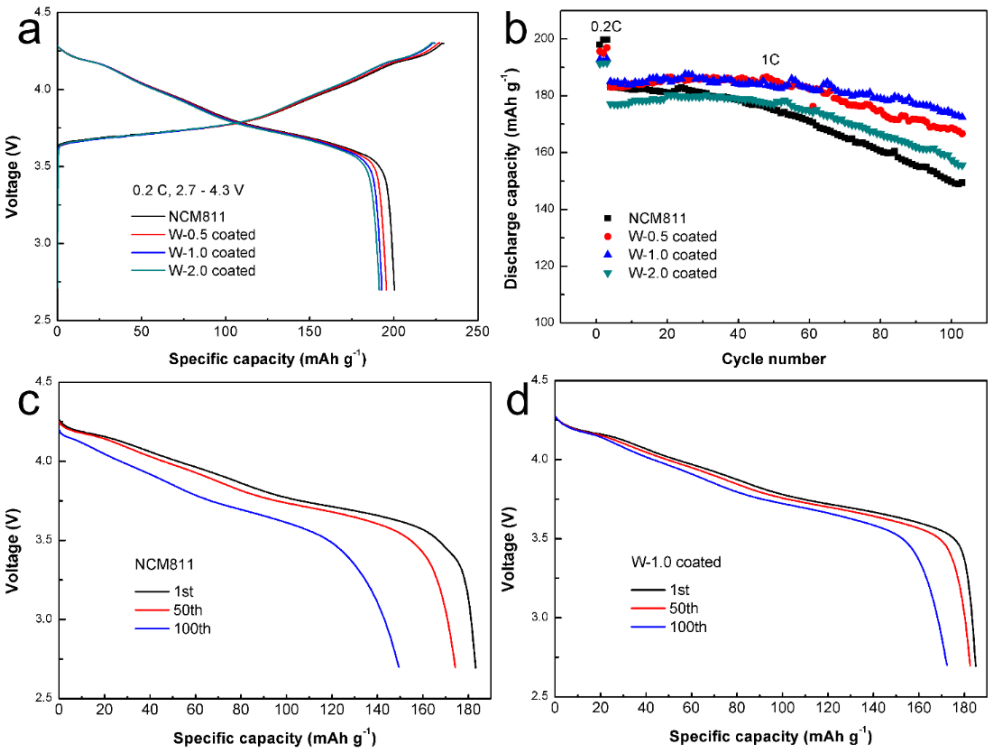

Figure 7. Initial charge-discharge curves (a) and the cycling performance (b) of NCM811 and WO_3 coated NCM811; The discharge curves at 1st, 50th, 100th cycle of NCM811 (c) and W-1.0 coated NCM811 (d).

Fig. 7a shows the first charge/discharge capacity curves for the four samples at 0.2 C. The all samples exhibit similar smooth charge/discharge curves, except for the differences in capacity, indicating that WO_3 coating does not hinder the insertion/extraction of Li^+ from the cathode materials. The first discharge capacities of 200.3, 195.6, 192.8 and 191.3 mAh g^{-1} are attained for NCM811, W-0.5, W-1.0 and W-2.0 coated NCM811 with first coulombic efficiencies of 87.2%, 86.0%, 86.0% and 85.5%, respectively. The initial discharge capacity and coulomb efficiency values gradually decrease as the proportion of WO_3 increases, which is related with the electrochemically stable W^{6+} species. The cycling performances of the cathode materials are shown in Fig. 7b, and Table 2 gives the results before and after 100 cycles for different samples. After 100 cycles at 1 C rate, the discharge capacities of NCM811, W-0.5, W-1.0 and W-2.0 coated NCM811 are 149.4, 166.7, 172.5 and 155.5 mAh g^{-1}, with capacity retention of 81.6%, 90.0%, 93.2% and 87.8% respectively. Fig. 7c and d show the discharge capacity of NCM811 and W-1.0 coated NCM811 is 183.2, 174.3, 149.4, 185.1 and 182.6, 172.5 mAh g^{-1} respectively, after 1, 50 and 100 cycles. It could be seen that the modified cathode material has higher discharge capacity and capacity retention than the unmodified one after 100 cycles. Notably, W-1.0 coated NCM811 exhibits the best cycling performance and discharge capacity compared to NCM811, W-0.5 coated NCM811 and W-2.0 coated NCM811. These results clearly reveal that WO_3 coating could effectively improve the electrochemical performances of NCM811cathode material.

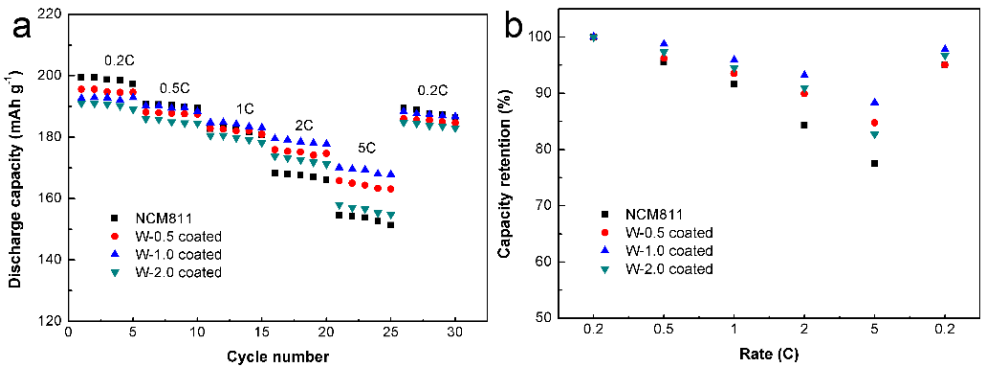

Figure 8. (a) Rate capability from 0.2 to 5.0 C rate, (b) Relative discharge capacity retention as a function of C-rate for the NCM811 and WO_3 coated NCM811.

Further study on the difference in the magnification properties of the unmodified and modified materials is shown in Fig. 8. The NCM811 has the highest discharge capacity at 0.2 C. However the discharge capacity of W-1.0 coated NCM811 exceeds that of NCM811 at 1 C rate. In particular, the discharge capacity of NCM811 is severely lost at current density of 5C, only having 151.3 mAh g^{-1} (the fifth circle) equivalent to 75.8% of the initial capacity. At the same conditions, compared with NCM811, W-1.0 coated NCM811 has a higher discharge capacity of 167.8 mAh g^{-1} (the fifth circle) and a higher capacity retention of 87.1%. Similarly, W-0.5 coated NCM811 has better rate performance than NCM811. Among the examined cathode materials, W-1.0 coated NCM811 displays the best rate performance. These experimental results further demonstrate that the WO_3 coating could enhance the surface structural stability during a long cycle and high rate charge/discharge process, and reduce the occurrence of side reactions between the electrolyte and the cathode material.

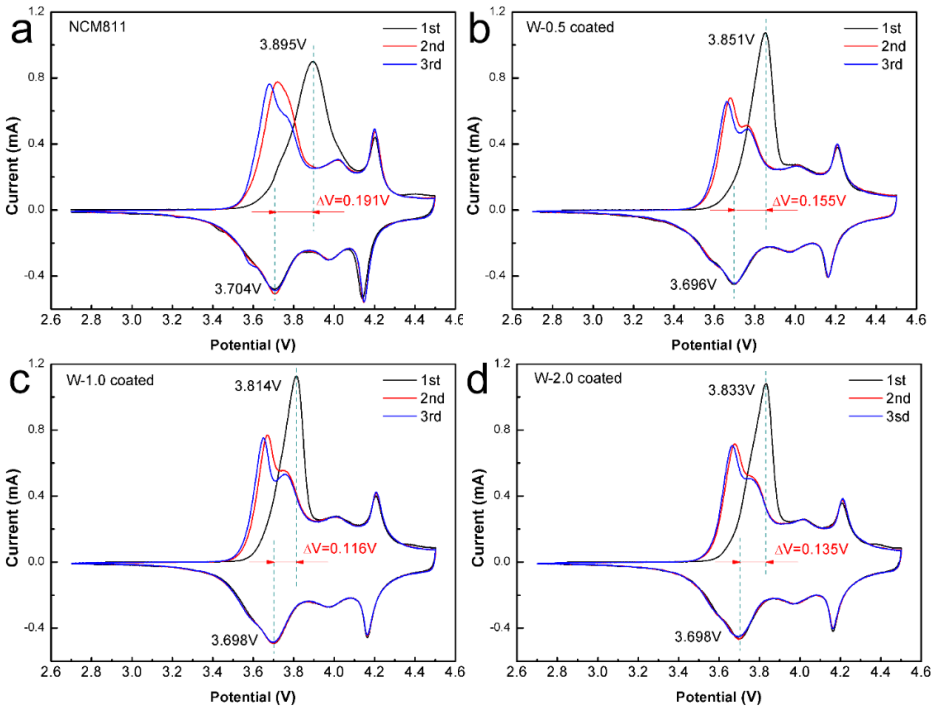

Figure 9. Cyclic voltammetry of NCM811 and WO_3 coated NCM811.

Table 2. Discharge parameters of NCM811 and WO_3 coated NCM811 at 1 C rate.

Sample	Discharge capacity ($mAh \cdot g^{-1}$)		Capacity retention (%)
	1st	100th	
NCM811	183.2	149.4	81.6
W-0.5 coated	183.1	166.7	91.0
W-1.0 coated	185.1	172.5	93.2
W-2.0 coated	177.1	155.5	87.8

The comparison between the present work and the previous investigation reported in the literature [32] is listed in Table 3. In comparison, the W-1.0 coated NCM811 has a higher discharge capacity (172.5 mAh g^{-1}) and better retention capacity (93.2%) than the 0.25 wt% WO_3 coated-NCM after 100 cycles in the potential rage of 2.7–4.3 V. In addition, the rate performance of W-1.0 coated NCM811 is also superior to that of the 0.25 wt% WO_3 coated-NCM at 0.2 C, 1 C and 5 C rate conditions

Table 3. Comparison with previous work

Ref.	Sample	Cycling performance			Rate performance		
		Discharge capacity ($mAh \cdot g^{-1}$)		Capacity retention (%)	Discharge capacity ($mAh \cdot g^{-1}$)		
		1st	100th		0.2 C	1 C	5 C
[32]	NCM[a]	180.8	146.8	81.2	193.1	179.6	144.5
	0.25wt % WO_3 coated-NCM	177.9	154.8	87.0	189.1	177.8	153.2
This work	NCM811	183.2	149.4	81.6	199.5	180.7	151.3
	1.0 wt% WO_3 coated-NCM811	185.1	172.5	93.2	192.6	183.0	167.8

[a] The NCM in the literature [32] is the same as NCM811 (i.e., $LiNi_{0.8}Co_{0.1}Mn_{0.1}O_2$).

To further analyze the electrochemical properties of the cathode material, the cyclic voltammetry tests (the initial three cycles) were performed on the all samples, as shown in Fig. 9. It is obvious that the all samples have a pair of distinct redox peaks in the potential range 3.6–3.9V, corresponding to Ni^{2+}/Ni^{3+} and Ni^{4+}. From Fig. 9, it could be seen that the oxidation and reduction peaks of NCM811, W-0.5, W-1.0 and W-2.0 coated NCM811 are 3.895 and 3.704 V, 3.851 and 3.696 V, 3.814 and 3.698 V, 3.833 and 3.698 V, respectively, and the corresponding potential differences (△Ep) between oxidation and reduction peaks are 0.191, 0.155, 0.116 and 0.135 V, respectively. As well known, the magnitude of the potential difference indicates the degree of polarization during the electrode reaction [39]. The results reveal that the WO_3 modification can reduce the polarization of NCM811 and improve the

reversibility of the electrode reaction. It is worth noting that W-1.0 coated NCM811 has the smallest potential difference, demonstrating that it has the best circulatory performance.

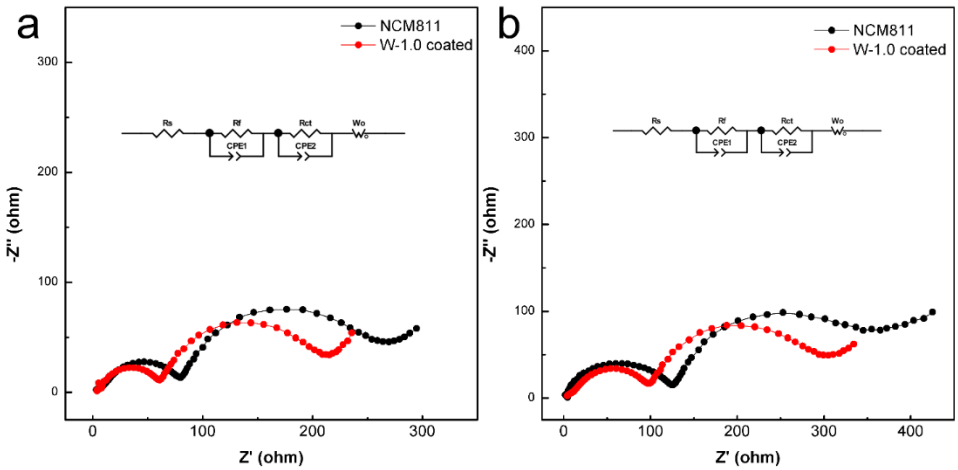

Figure 10. Nyquist plots of NCM811 and W-1.0 coated NCM811 at a discharge state: before discharge (a) and after 100 cycles (b).

Table 4. Fitted impedance parameters of NCM811 and W-1.0 coated NCM811 at different cycles.

Sample	Cycles	R_s (Ω)	R_f (Ω)	R_{ct} (Ω)
NCM811	0th	6.5	66.8	151.2
	100th	6.9	111.6	243.2
W-1.0 coated	0th	4.6	40.0	133.0
	100th	6.1	82.6	165.5

EIS experiments were performed on NCM811 and W-1.0 coated NCM811 in the discharge state to further examine the effect of WO_3 coating on the kinetic behaviour of NCM811. As shown in Fig. 10, the impedance spectra of these samples are similar in shape. R_s, R_f, and R_{ct} represent the resistance of the electrolyte solution, the resistance of the SEI membrane, and the charge transfer resistance of the electrode interface with the electrolyte, respectively [40, 41]. The results obtained by fitting the impedance spectra were listed in Table 4. After 100 cycles, the R_s of NCM811 and W-1.0 coated NCM811 was very close. However, the R_f value of W-1.0 coated NCM811 increased from 40.0 to 82.6 Ω, while the R_f value of NCM 811 increased from 66.8 to 111.6 Ω. This may be due to the modification of WO_3 reducing the thickness of the SEI film. Notably, the R_{ct} increasing value of W-1.0 coated NCM811 is much smaller than that of NCM811 after 100 cycles, indicating that the WO_3 coating could

effectively inhibit the cathode material to be destroyed by HF and side reactions, and maintain the structural stability of the cathode material.

4. CONCLUSIONS

In summary, WO_3-coated $LiNi_{0.8}Co_{0.1}Mn_{0.1}O_2$ cathode material was smoothly prepared via a wet-chemical coating route. Various tests have indicated that WO_3 forms a dense protective layer on the surface of $LiNi_{0.8}Co_{0.1}Mn_{0.1}O_2$, and a small amount of W^{6+} could enter to the lattice of $LiNi_{0.8}Co_{0.1}Mn_{0.1}O_2$. The WO_3 coating can greatly enhance the cycling performance and rate performance of $LiNi_{0.8}Co_{0.1}Mn_{0.1}O_2$. The 1.0 wt% WO_3 coated $LiNi_{0.8}Co_{0.1}Mn_{0.1}O_2$ displays the best electrochemical performances compared to other samples with different coating amounts of WO_3 and the unmodified $LiNi_{0.8}Co_{0.1}Mn_{0.1}O_2$. With the WO_3 modification, the capacity retention of $LiNi_{0.8}Co_{0.1}Mn_{0.1}O_2$ was significantly increased from 81.6% to 93.2% after 100 cycles at 1 C. It could be concluded that the WO_3 coating can reduce the degree of polarization during the electrochemical reaction of $LiNi_{0.8}Co_{0.1}Mn_{0.1}O_2$, and inhibit the corrosion of HF and side reactions for the cathode material, thus keeping structural stability of $LiNi_{0.8}Co_{0.1}Mn_{0.1}O_2$.

ACKNOWLEDGEMENTS
This work was supported by the National Natural Science Foundation of China (21572070), and the Technological Innovation and Development Project of Guangdong Province ([2018] No. 379).

References

1. L. Peng, Y. Zhu, U. Khakoo, D. Chen, G. Yu, *Nano Energy*, 17 (2015) 36.
2. Y. Cho, P. Oh, J. Cho, *Nano Lett.*, 13 (2013) 1145.
3. D. Wang, R. Kou, Y. Ren, C.-J. Sun, H. Zhao, M.-J. Zhang, Y. Li, A. Huq, J. Y. P. Ko, F. Pan, Y.-K. Sun, Y. Yang, K. Amine, J. Bai, Z. Chen, F. Wang, *Adv. Mater.*, 29 (2017).
4. C. Fu, G. Li, D. Luo, Q. Li, J. Fan, L. Li, *ACS Appl. Mater. Interfaces*, 6 (2014) 15822.
5. J.-H. Shim, J.-S. Im, H. Kang, N. Cho, Y.-M. Kim, S. Lee, *J. Mater. Chem. A*, 6 (2018) 16111.
6. D.-H. Cho, C.-H. Jo, W. Cho, Y.-J. Kim, H. Yashiro, Y.-K. Sun, S.-T. Myung, *J. Electrochem. Soc.*, 161 (2014) A920.
7. J. Xu, S. Dou, H. Liu, L. Dai, *Nano Energy*, 2 (2013) 439.
8. W. Liu, P. Oh, X. Liu, M.-J. Lee, W. Cho, S. Chae, Y. Kim, J. Cho, *Angew. Chem. Int. Ed.*, 54 (2015) 4440.
9. S. Gao, X. Zhan, Y.-T. Cheng, *J. Power Sources*, 410–411 (2019) 45.
10. Z. Huang, Z. Wang, H. Guo, X. Li, *J. Alloys Compd.*, 671 (2016) 479.
11. D. Wang, Z. Wang, X. Li, H. Guo, Y. Xu, Y. Fan, W. Pan, *Appl. Surf. Sci.*, 371 (2016) 172.
12. J. Yang, B. Huang, J. Yin, X. Yao, G. Peng, J. Zhou, X. Xu, *J. Electrochem. Soc.*, 163 (2016) A1530.
13. C. Hua, K. Du, C. Tan, Z. Peng, Y. Cao, G. Hu, *J. Alloys Compd.*, 614 (2014) 264.
14. Y. K. Sun, S. T. Myung, M. H. Kim, J. Prakash, K. Amine, *J. Am. Chem. Soc.*, 127 (2005) 13411.
15. Y. Su, S. Cui, Z. Zhuo, W. Yang, X. Wang, F. Pan, *ACS Appl. Mater. Interfaces*, 7 (2015) 25105.
16. X. Xiong, Z. Wang, H. Guo, Q. Zhang, X. Li, *J. Mater. Chem. A*, 1 (2013) 1284.
17. F. Ma, Y. Wu, G. Wei, S. Qiu, J. Qu, *J. Solid State Electrochem.*, 23 (2019) 2213.
18. D. Li, Y. Kato, K. Kobayakawa, H. Noguchi, Y. Sato, *J. Power Sources*, 160 (2006) 1342.

19. J. Cho, T. J. Kim, Y. J. Kim, B. Park, *Electrochem Solid St*, 4 (2001) A159.
20. J. Huang, X. Fang, Y. Wu, L. Zhou, Y. Wang, Y. Jin, W. Dang, L. Wu, Z. Rong, X. Chen, X. Tang, *J. Electroanal. Chem.*, 823 (2018) 359.
21. L. Song, F. Tang, Z. Xiao, Z. Cao, H. Zhu, A. Li, *J. Electron. Mater.*, 47 (2018) 5896.
22. X. Xiong, D. Ding, Z. Wang, B. Huang, H. Guo, X. Li, *J. Solid State Electrochem*., 18 (2014) 2619.
23. Q. Y. Wang, J. Liu, A. V. Murugan, A. Manthiram, *J Mater Chem*, 19 (2009) 4965.
24. Z.-F. Tang, R. Wu, P.-F. Huang, Q.-S. Wang, C.-H. Chen, *J. Alloys Compd*., 693 (2017) 1157.
25. P. Yue, Z. Wang, H. Guo, X. Xiong, X. Li, *Electrochim. Acta*, 92 (2013) 1.
26. J. Zheng, M. Gu, J. Xiao, B. J. Polzin, P. Yan, X. Chen, C. Wang, J.-G. Zhang, *Chem. Mater.*, 26 (2014) 6320.
27. S. Dai, G. Yan, L. Wang, L. Luo, Y. Li, Y. Yang, H. Liu, Y. Liu, M. Yuan, *J. Electroanal. Chem*., 847 (2019).
28. W. Liu, X. Li, D. Xiong, Y. Hao, J. Li, H. Kou, B. Yan, D. Li, S. Lu, A. Koo, K. Adair, X. Sun, *Nano Energy*, 44 (2018) 111.
29. C. Yuan, H. Lin, H. Lu, E. Xing, Y. Zhang, B. Xie, *Mater. Lett.*, 148 (2015) 167.
30. K. Mu, Y. Cao, G. Hu, K. Du, H. Yang, Z. Gan, Z. Peng, *Electrochim. Acta*, 273 (2018) 88.
31. G. Song, H. Zhong, Y. Dai, X. Zhou, J. Yang, *Ceram. Int.*, 45 (2019) 6774.
32. Z. Gan, G. Hu, Z. Peng, Y. Cao, H. Tong, K. Du, *Appl. Surf. Sci.*, 481 (2019) 1228.
33. K. Yang, L.-Z. Fan, J. Guo, X. Qu, *Electrochim. Acta*, 63 (2012) 363.
34. S. K. Martha, H. Sclar, Z. S. Framowitz, D. Kovacheva, N. Saliyski, Y. Gofer, P. Sharon, E. Golik, B. Markovsky, D. Aurbach, *J. Power Sources*, 189 (2009) 248.
35. Z. Chen, Y. Liu, Z. Lu, R. Hu, J. Cui, H. Xu, Y. Ouyang, Y. Zhang, M. Zhu, *J. Alloys Compd.*, 803 (2019) 71.
36. Y. Baek, K. Yong, *J. Phys. Chem.* C, 111 (2007) 1213.
37. D. Lv, L. Wang, P. Hu, Z. Sun, Z. Chen, Q. Zhang, W. Cheng, W. Ren, L. Bian, J. Xu, A. Chang, *Electrochim. Acta*, 247 (2017) 803.
38. G. Shang, Y. Tang, Y. Lai, J. Wu, X. Yang, H. Li, C. Peng, J. Zheng, Z. Zhang, *J. Power Sources*, 423 (2019) 246.
39. J. Ahn, E. K. Jang, S. Yoon, S.-J. Lee, S.-J. Sung, D.-H. Kim, K. Y. Cho, *Appl. Surf. Sci.*, 484 (2019) 701.
40. S. H. Ju, I.-S. Kang, Y.-S. Lee, W.-K. Shin, S. Kim, K. Shin, D.-W. Kim, *ACS Appl. Mater. Interfaces*, 6 (2014) 2546.
41. J. Ahn, S. Yoon, S. G. Jung, J.-H. Yim, K. Y. Cho, *J. Mater. Chem. A*, 5 (2017) 21214.